

Force-induced activation of Talin and its possible role in focal adhesion mechanotransduction

Seung E. Lee^a, Roger D. Kamm^{a,b}, Mohammad R.K. Mofrad^{c,*}

^aDepartment of Mechanical Engineering, Massachusetts Institute of Technology, Cambridge, MA 02139, USA

^bBiological Engineering Division, Massachusetts Institute of Technology, Cambridge, MA 02139, USA

^cMolecular Cell Biomechanics Laboratory, Department of Bioengineering and Graduate Group in Biophysics, University of California, Berkeley, CA 94720, USA

Accepted 10 April 2007

Abstract

It is now well established that cells can sense mechanical force, but the mechanisms by which force is transduced into a biochemical signal remain poorly understood. One example is the recruitment of vinculin to reinforce initial contacts between a cell and the extracellular matrix (ECM) due to tensile force. Talin, an essential linking protein in an initial contact, contains at least one vinculin-binding site (VBS) that is cryptic and inactive in the native state. The N-terminal five-helix bundle of talin rod is a stable structure with a known cryptic VBS1. The perturbation of this stable structure through elevated temperature or destabilizing mutation activates vinculin binding. Although the disruption of this subdomain by transmitted mechanical force is a potential cue for the force-induced focal adhesion strengthening, the molecular basis for this mechanism remains elusive. Here, molecular dynamics (MD) is employed to demonstrate a force-induced conformational change that exposes the cryptic vinculin-binding residues of VBS1 to solvent under applied force along a realistic pulling direction. VBS1 undergoes a rotation of $62.0 \pm 9.5^\circ$ relative to its native state as its vinculin-binding residues are released from the tight hydrophobic core. Charged and polar residues on the VBS1 surface are the site of force transmission that strongly interact with an adjacent α -helix, and in effect, apply torque to the VBS1 to cause its rotation. Activation was observed with mean force of 13.2 ± 8.0 pN during constant velocity simulation and with steady force greater than 18.0 pN.

© 2007 Elsevier Ltd. All rights reserved.

Keywords: Mechanotransduction; Talin; Vinculin; Focal adhesion

1. Introduction

Living cells respond to mechanical stimulation in a variety of ways that shape their phenotype in health and disease. Although the biochemical signaling pathways activated by mechanical stimuli have been extensively studied, little is known of the basic mechanisms. One hypothesis is that forces transmitted via individual proteins either at the site of cell adhesion to its surroundings or within the stress-bearing members of the cytoskeleton cause conformational changes that alter their binding affinity to other intracellular molecules. This altered equilibrium state can subsequently initiate a biochemical

signaling cascade or produce more immediate and local structural changes; see reviews (Kamm and Kaazempur-Mofrad, 2004; Vogel, 2006; Vogel and Sheetz, 2006). Several examples have been proposed to support this hypothesis; see e.g. the study of mechanosensitive ion channels (Sotomayor and Schulten, 2004) and steered molecular dynamics (MD) of fibronectin (Gao et al., 2002). Yet, the mechanism by which intracellular proteins are activated by force remains open to debate.

One key mechanosensing protein in focal adhesions is talin, a cytoplasmic protein with a globular head and an elongated rod that provides an essential structural link between integrins and the actin cytoskeleton (Critchley, 2000). The globular head of talin binds to β -integrin (Calderwood, 2004) and can also bind to and activate phosphatidylinositol 4 phosphate 5-kinase type γ (PIP2- γ)

*Corresponding author. Tel.: +1 510 643 8165; fax: +1 510 642 5835.
E-mail address: mofrad@berkeley.edu (M.R.K. Mofrad).

(Di Paolo et al., 2002; Ling et al., 2002). This, in turn, locally increases the production of phosphatidylinositol 4,5 bisphosphate (PIP2) (Ling et al., 2002), which is known to activate a number of focal adhesion proteins (e.g. vinculin and talin), hence promoting focal adhesion assembly (Ling et al., 2002). The talin rod can bind to β -integrin (Xing et al., 2001) and F-actin (Hemmings et al., 1996), and contains 11 vinculin-binding sites (VBSs), each of which is an amphipathic α -helix (Bass et al., 1999; Gingras et al., 2006). Vinculin is a cytoplasmic protein that may function as a structural reinforcement. It consists of a globular head, a proline-rich neck region, and a rod-like tail domain, which contains binding sites for many other cytoplasmic proteins (Winkler et al., 1996; Bakolitsa et al., 1999). Cells with disrupted talin function fail to form focal adhesions and exhibit spreading defects (Priddle et al., 1998). Cells with vinculin disruption, however, can still form focal adhesions, but display reduced ability to spread and increased cell motility (Xu et al., 1998).

Since mechanical force is needed for vinculin recruitment to focal adhesions (Galbraith et al., 2002), force-induced activation of cryptic VBSs on talin through conformational change may be the mechanosensing pathway leading to recruitment (Vogel, 2006). Such recruitment could also lead to reinforcement of the focal adhesion. Indeed, talin1 is critical in force-dependent vinculin recruitment to adhesion sites independent of Src family kinase and focal adhesion kinase activities (Giannone et al., 2003). Jiang et al. (2003) identified that the initial contact that a cell makes with the extracellular matrix (ECM) consists of ECM-integrin-talin-F-actin linkages.

Some of the talin VBSs are inactive and unable to bind to the vinculin subdomain (Vh1; residues 1–258) (Patel et al., 2006). Vh1 is a subdomain of vinculin head that contains the binding site for talin and is used in various talin-binding experiments (Izard et al., 2004; Patel et al., 2006). The first vinculin-binding site (VBS1; residues 606–636) is the fourth helix (H4) of a stable N-terminal five-helix bundle (TAL5) of talin rod (Papagrigoriou et al., 2004). VBS1 has hydrophobic residues that, upon binding to Vh1, become deeply embedded in a hydrophobic core of the Vh1 (Izard et al., 2004). The same vinculin-binding residues form a tight hydrophobic core within TAL5 (Papagrigoriou et al., 2004). Experiments have shown that isolated TAL5 has a low binding affinity for Vh1, whereas a four-helix bundle with helix-5 (H5) removed from TAL5 (Patel et al., 2006), a mutated TAL5 with an unstable hydrophobic core (Papagrigoriou et al., 2004), or the wild-type TAL5 molecule in elevated temperature solvent (Patel et al., 2006) can each disrupt TAL5 stability and strongly bind to Vh1.

MD has been used to study the force response on various molecular structures (Lu et al., 1998; Gao et al., 2002; Carrion-Vazquez et al., 2003). Mostly, unfolding pulling forces were applied between two atoms (e.g. C- and N-termini), and the results were compared with the corresponding Atomic Force Microscopy (AFM) experi-

ments (Marszalek et al., 1999; Oberhauser et al., 2002). The unfolding force applied on fibronectin causes its cryptic binding site to get exposed to the solvent (Gao et al., 2002). However, the force being transmitted within a typical force-bearing intracellular protein is likely to be through the hydrogen bonds between secondary structures rather than through the termini. Indeed, the applied force through the termini is transmitted through the hydrogen bonds between the β -sheets, and force drops are observed as these hydrogen bonds are broken (Lu et al., 1998; Gao et al., 2002). However, no MD studies with realistic force application on the secondary structures were reported.

Here, using computational methods, we demonstrate that realistically transmitted force acting on the focal adhesion protein talin leads to a conformational change that exposes the cryptic vinculin-binding residues of VBS1. This then enables force-induced recruitment of vinculin, a critical early step in the process of focal adhesion reinforcement. Sequence homology of VBS1 with other VBSs suggests that the proposed mechanism may be a general force-induced activation mechanism of cryptic VBSs, and perhaps even be one of the general mechanotransduction mechanisms of helical bundles.

2. Methods

2.1. TAL5 simulation with EEF1

The structure of TAL5 was obtained by removing the C-terminal four-helix-bundle from TAL9 (PDB ID: 1SJ8) (Papagrigoriou et al., 2004). The location and the assumed orientation of TAL9 within talin are shown in Fig. 1A. The longest principal length of TAL5 is aligned along the y-axis and the cross product of the vectors along H1 and H5 is aligned along the z-axis (Fig. 1B). Commercial molecular dynamics software, CHARMM (Harvard University, Cambridge, MA) (Brooks et al., 1983), was used with Effective Energy Function (EEF1) (Lazaridis and Karplus, 1999) solvent model and the CHARMM19 force field (Neria et al., 1996). The crystal structure was minimized by alternating the Steepest Decent and Adopted Basis Newton Raphson methods with 3000 steps. Bond lengths between hydrogen and heavy atoms were fixed using SHAKE constraint (Krautler et al., 2001), and a 2fs time step was used. Heating of the molecule to 300 K occurred over 40 ps, followed by a 560 ps equilibration period at 300 K.

Umbrella sampling (Torrie, 1974) module of CHARMM with parabolic potential force constant of 5.0 kcal/mol-Å² imposed on the reference reaction coordinates. One atom of each of the four residues of H5 (Q635, Q646, E650, and Q653) was harmonically constrained in space ($k = 0.2$ kcal/mol-Å²). Forces were applied along a reaction coordinate defined as distance along a line from the center of mass of the H1 atom selection (side chain atoms of T498, S501, and S502) to a dummy atom with neutral charge and no mass located at coordinate (25.0, -17.0, 4.0 Å) (Fig. 1B). At each reference distance separated by 0.1 Å, an 800 ps canonical ensemble calculation was performed with Nosé-Hoover (Nosé, 1984; Hoover, 1985) thermostat for constant temperature control at 300 K. Nuclear-Oberhauser-Effect (NOE) constraints were imposed to the backbone hydrogen bonding pairs within H1 to prevent unraveling. In order to start the simulations with intact VBS1–H1 interaction, NOE constraints were imposed to polar sidechains between VBS1 and H1 during equilibration, which were removed at the beginning of the production runs. It should be noted that the sequential stepping (0.1 Å) used is smaller than the fluctuation along the reaction coordinate around the reference value ($\sim \pm 1$ Å), and therefore, the trajectory from the umbrella sampling simulation is similar to a constant velocity MD

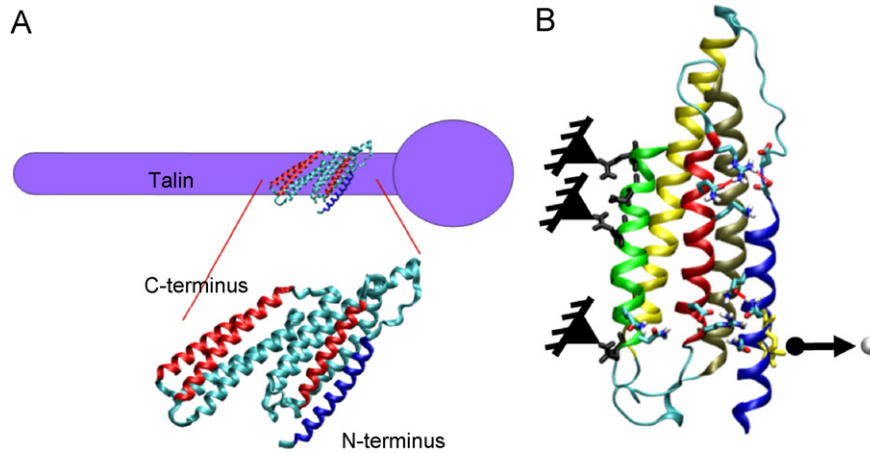


Fig. 1. (A) Crystal structure of TAL9 (PDB ID: 1SJ8) in ribbon representation is shown superimposed on a hypothetical talin model. Three VBSs within TAL9 are shown in red, and H1 is shown in blue. Since the talin rod has tandem repeats of helical bundles, TAL9 is aligned such that the centers of mass of the two helical bundles lie on the talin rod axis. (B) Detailed view of the N-terminal five-helix bundle (TAL5) used in the TAL5 simulations. Each of the five helices is shown in a different color: H1 (blue), H2 (yellow), H3 (tan), H4 (or VBS1; red), and H5 (green). Some important polar residues are shown in stick representations. A dummy atom with no mass or charge is shown in white. H5 polar side chains (black sticks) are harmonically constrained in space (constraints shown as triangles). H1 polar side chains (yellow sticks) are pulled toward the dummy atom (effective pulling direction shown as an arrow).

calculation (Izrailev et al., 1999) with effective pulling velocity of 0.125 \AA/ns .

Constant force simulations with force magnitude varying between $F = 15.0$ to 25.0 pN were performed using the same TAL5 model described above. Constant force of $F/(\text{no. of atoms on which the force is applied})$ was applied to each of the side chain atoms on H1 (T498, S501, and S502) toward the positive x-direction, such that total force applied is F .

2.2. Mutational study on TAL5

Three mutated TAL5 structures were constructed using the MMTSB toolset (Feig et al., 2004): (i) H5 residues N636 and Q639 mutated to alanines; (ii) VBS1 residues R606, Q610, K613, E621 and R624 all mutated to alanines; (iii) H1 residues N500, Q504, Q507, D514, and D515 all mutated to alanines. Umbrella sampling simulations identical to those described above are performed on each mutated structure.

2.3. Explicit water simulation on TAL5

TAL5 was solvated in an orthorhombic solvent box with each face at least 10 \AA away from TAL5 resulting in 23,775 atoms. Periodic boundary conditions were imposed using the image module. Electrostatic charge of the solvated system was neutralized by replacing seven water molecules with sodium ions. An all-hydrogen representation was used with CHARMM27 force fields (MacKerell et al., 1998). The SHAKE constraint and 2fs time steps was used. SHIFT truncation was imposed with a cutoff distance of 12 \AA for non-bonded interactions, which has been found to exhibit reasonable accuracy in explicit water simulations (Beck et al., 2005). Long range non-bonded interactions, beyond the cutoff distance, were not taken into account in our explicit water simulations. The model was thoroughly minimized. The system was heated to 300 K in 40 ps and equilibrated for 960 ps. An umbrella sampling potential of $5.0 \text{ kcal/mol-\AA}^2$ was used. H5 sidechain atoms (Q646, E650, and Q653) were harmonically constrained with force constant of $1.5 \text{ kcal/mol-\AA}^2$. Using a reference distance step size of 0.2 \AA , and 400 ps simulation at each step a canonical ensemble simulation was performed with Nosé-Hoover at each reference distance, which is equivalent to 0.5 \AA/ns pulling rate. A constant force simulation with $F = 50.0 \text{ pN}$ was also performed. All

explicit solvent simulations were performed on DataStar IBM p655 at San Diego Supercomputing Center (SDSC).

3. Results

TAL5 forms a stable structure with cryptic VBS1, which cannot bind to Vh1 in intact TAL5, but elevated temperature can effectively disrupt its stability and allow it to strongly bind to Vh1 (Patel et al., 2006). Explicit water simulations at 300, 360, and 420 K were performed to investigate what constitutes TAL5 stability and the destabilizing effects of elevated temperature. Hydrophobic residues of H5 (L651, A647, V644, and A640) form a tight groove-fitting interaction with hydrophobic residues of VBS1 (A611, L615, A618, and L622) (Fig. 2). This interaction prevents VBS1 hydrophobic residues, which are the vinculin-binding residues, from becoming exposed to the solvent. The trajectories of elevated temperature simulations (360 and 420 K) did not differ much from those at room temperature (300 K) other than the expected increase in thermal fluctuation. The RMSD of backbone atoms from crystal structures and average distances with fluctuations of VBS1-H1, VBS1-H2, VBS1-H3, and VBS1-H5 for three simulations are shown in Table 1. H5 and H3 closely interact with VBS1, and with other helices to a lesser extent (Fig. 2B). It is likely that this interaction must be disrupted in elevated temperature or force-induced activation of VBS1.

In the TAL5 simulations displaying VBS1 activation, the hydrophobic residues of VBS1 (L608, L609, L615, V619, L622, and L623) form a tight hydrophobic core with the hydrophobic residues of H3 (V577, I580, L584, M587, V591, and L594) and the hydrophobic residues of H5 (L637, A640, V644, A647, L651, and I655) before

extension. Polar and charged residues on VBS1 interact with H1 and H5 through hydrogen bonds and salt bridges. RQK (R606, Q610, and K613) cluster on VBS1 interacts strongly with H1 (D514 and D515) by forming salt bridges (Figs. 1B and 3B). ER (E621 and R624) cluster on VBS1 interacts with H5 (N636 and Q639) and more strongly with H1 (N500, Q504, and Q507) as N500, Q504, and Q507 of H1 surround and form hydrogen bonds with R624 of VBS1 (Figs. 1B and 3B). As force is applied to TAL5, it is transmitted through these hydrogen bonds. Since VBS1-H1 interaction is stronger, the transmitted force applies a torque through the RQK and ER clusters on VBS1 and the VBS1-H5 interaction is broken. As shown in Fig. 3, the hydrophobic contact formed by VBS1 with H3 and H5 eventually slips, and the hydrophobic residues of VBS1 are exposed to the solvent as VBS1 undergoes a rigid body rotation (Fig. 3B and D). The hydrophobic residues of H5 fit into the V-shaped groove of VBS1 as one side of the ‘V’ (L608, L615, and L622) gets exposed to the solvent and the other side (L609, V619, and L623) forms a new hydrophobic core with H5 and H3 (Fig. 3C and D) (Supplementary Movies 1, 2 and 3).

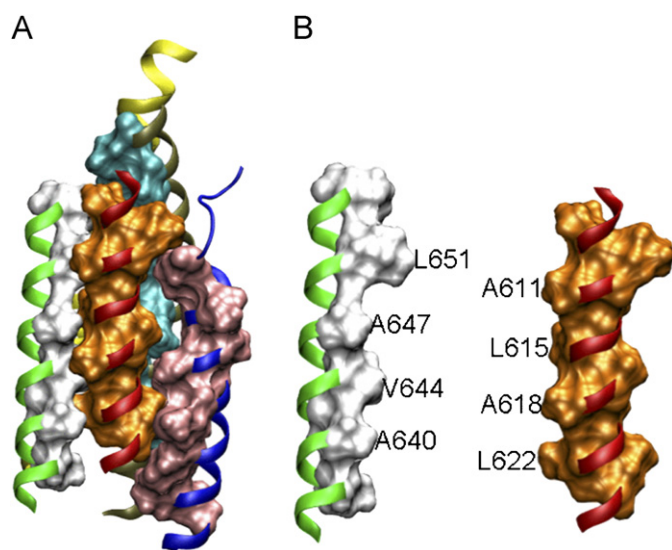


Fig. 2. (A) TAL5 in the same orientation as Figure 1B with hydrophobic residues shown in surface representation for H1 (pink), H3 (cyan), VBS1 (orange), and H5 (white). Exposed ribbon sites are polar residues, whose side chains are not shown for clarity. VBS1 and H5 form a tight groove-fitting contact, which stabilizes VBS1 in TAL5's hydrophobic core preventing VBS1 from being accessible for vinculin binding. (B) VBS1 and H5 are shown separately with labels for residues participating in the groove-fitting interaction.

Table 1

RMSD from crystal structure and average distances between helices from elevated temperature explicit water simulations

	Distance between VBS1-H1 (Å)	Distance between VBS1-H2 (Å)	Distance between VBS1-H3 (Å)	Distance between VBS1-H5 (Å)	RMSD (Å)
$T = 300\text{ K}$	14.03 ± 0.26	14.38 ± 0.25	10.46 ± 0.21	8.04 ± 0.20	1.9635
$T = 360\text{ K}$	13.79 ± 0.26	14.43 ± 0.25	10.57 ± 0.20	8.10 ± 0.20	2.3258
$T = 420\text{ K}$	13.51 ± 0.35	14.33 ± 0.28	10.86 ± 0.26	8.44 ± 0.24	2.7919

Solvent accessible surface area (SASA) of the hydrophobic residues of VBS1 (Fig. 4A, D, and G) show how much of these residues are exposed. The extent of VBS1 rotation is shown by measuring the angle made by L622 (only selected as a reference, which is within the hydrophobic core of TAL5 and gets exposed to solvent later) with the vector connecting the centers of mass of VBS1 and H5 (Fig. 4B, E, and H; angle definition in Fig. 5). VBS1 activation is defined by L622 angle becoming negative, since this is the clearest measure of helix rotation to expose VBS1 for possible binding. An increase in SASA is also indicative of activation, although this measure is also influenced by exposure of VBS1 residues internally, caused by H1 peeling away from VBS1. Note that the force peaks (Fig. 4C) are sharp, but the corresponding changes in rotation angle are more gradual and tend to lag behind the reduction in force. This may be due to rotation being diffusive in nature, occurring subsequent to the drop in force impeding rotation. Results from two VBS1 activated simulations and one non-activated simulation (for comparison) is shown in Fig. 4. By visual inspection on the VBS1 rotation plots displaying negative angles (e.g. Fig. 4B, E, and H), 71.4% of the TAL5 simulations ($n = 20$ out of 28) exhibited the VBS1 activation. Analyzing only the simulations with VBS1 activation, $157.5 \pm 70.9 \text{ \AA}^2$ of hydrophobic SASA of VBS1 was exposed to solvent, VBS1 rotated by $62.0 \pm 9.5^\circ$, and a mean force of $13.2 \pm 8.0 \text{ pN}$ was required for activation.

Activation of VBS1 follows disruption of the tight hydrophobic interaction of VBS1 with H3 and H5 rather than resulting from hydrogen-bond breakage. Rotation due to the applied torque through RQK and ER handles is opposed by the hydrophobic contacts from H3 and H5 (Fig. 6). Non-bonded components of the interaction force on the hydrophobic sidechains of H3 and H5 experience force drops that correspond to the yielding of VBS1 to rotation (Fig. 6B). The identified sidechains opposing VBS1 rotation exhibit simultaneous drops in force magnitude near 2 ns. Time traces of the non-bonded force on A640, L651, L584, and V591 are shown in the subset of Fig. 6B (Supplementary Movie 4).

4. Discussion and conclusion

VBS1 activation in TAL5 is triggered by torque transmitted through the RQK and ER handles (Fig. 3A and B). Polar side groups of H5 (N636 and Q639) oppose VBS1 activation by stabilizing the non-extended TAL5

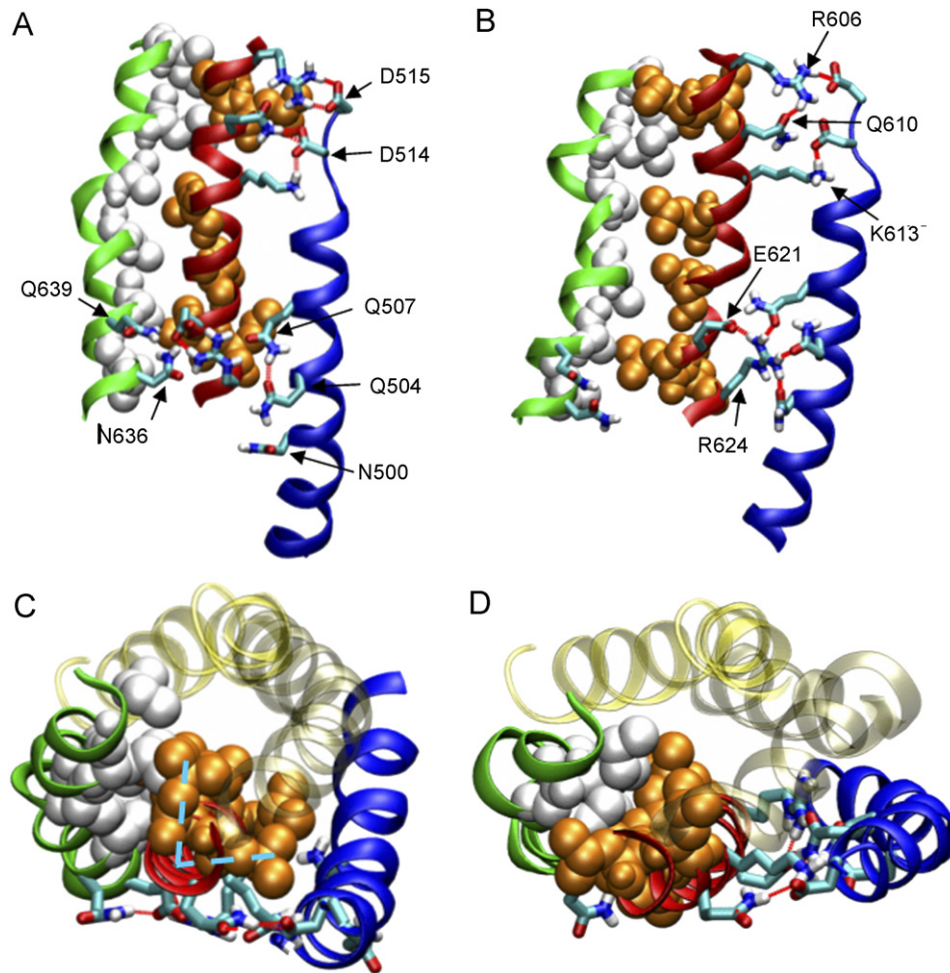


Fig. 3. Conformations showing VBS1 activation from the TAL5 simulation: H1 (blue ribbon), H2 (transparent yellow), H3 (transparent tan), VBS1 (red ribbon), H5 (green ribbon), hydrophobic residues of VBS1 (orange VDW; also the vinculin-binding residues), hydrophobic residues of H5 (white VDW), and some important polar residues (stick representation with color denoting the atom type). Polar residues are labeled on the figures. (A) Conformation at $t = 2.08$ ns. The hydrophobic residues of VBS1 (orange VDW) are hidden in the hydrophobic core. (B) Conformation at $t = 7.40$ ns showing the hydrophobic residues of VBS1 being exposed to solvent. Hydrogen bonds between H5 and VBS1 are broken. The hydrophobic residues, or the vinculin-binding residues, point into the page in (A) and point to left in (B). (C) Conformation at $t = 0.86$ ns viewed from top. The V-shaped VBS1 hydrophobic residues are packed within the hydrophobic core of TAL5 (cyan dotted lines). (D) Conformation at $t = 9.24$ ns showing VBS1 rotation. The hydrophobic residues H5 (white VDW) fit into the 'V' of the VBS1 hydrophobic residues (orange VDW).

structure. Indeed, in simulations that did not undergo VBS1 activation, the ER handle formed hydrogen bonds with H5 after breaking the hydrogen bonds with H1. This, however, did not cause VBS1 rotation in the opposite direction, suggesting that VBS1 activation can only occur when VBS1 forms strong hydrogen bonds with H1. Simulations on three mutated structures were performed to verify the role of polar side chains on H1, VBS1, and H5. Simulation with H5 mutation (N636 and Q639 to alanines) enhanced VBS1 activation, whereas VBS1 mutation (RQK and ER are all mutated to alanines) and H1 mutation (N500, Q504, Q507, D514, and D515 mutated to alanines) impaired VBS1 activation, all consistent with our argument (data not shown).

Interestingly, the RQK and ER handles or similar motifs are ubiquitous in talin rod VBSs suggesting this mechanism as a general force-induced VBS activation mechanism of talin. For example, VBS2 (residues 852–876) contains

sequences (**K**ILAD and **K**MV**E**AAK) (Bass et al., 1999) similar to ER (**E**LLR) and RQK (**R**PLL**Q**AAK) handles of VBS1 in terms of charges. Also, VBS3 (residues 1944–1969) contains (**K**KE**L**IECARR**V**s**E**K) (Bass et al., 1999). Charged and polar residues are shown in bold face to highlight the similarity with ER and RQK sequences of VBS1. Another protein, α -actinin, localizes to cell–cell and cell–matrix junctions. Similar to talin, α -actinin has an amphipathic α -helix (α VBS; residues 731–760) that can also bind to the same binding site on Vh and contains a sequence (**R**TINE) (Bois et al., 2005) similar to the ER handle of talin VBS1. As the vinculin-binding residues of α VBS are also cryptic in an intact α -actinin structure (Ylanne et al., 2001), it is possible that α -actinin may be another force-sensitive protein, which gets activated by a similar mechanism, in vinculin recruitment.

The EEF1 model used in this study is empirically based method characterized by high efficiency (Lazaridis and

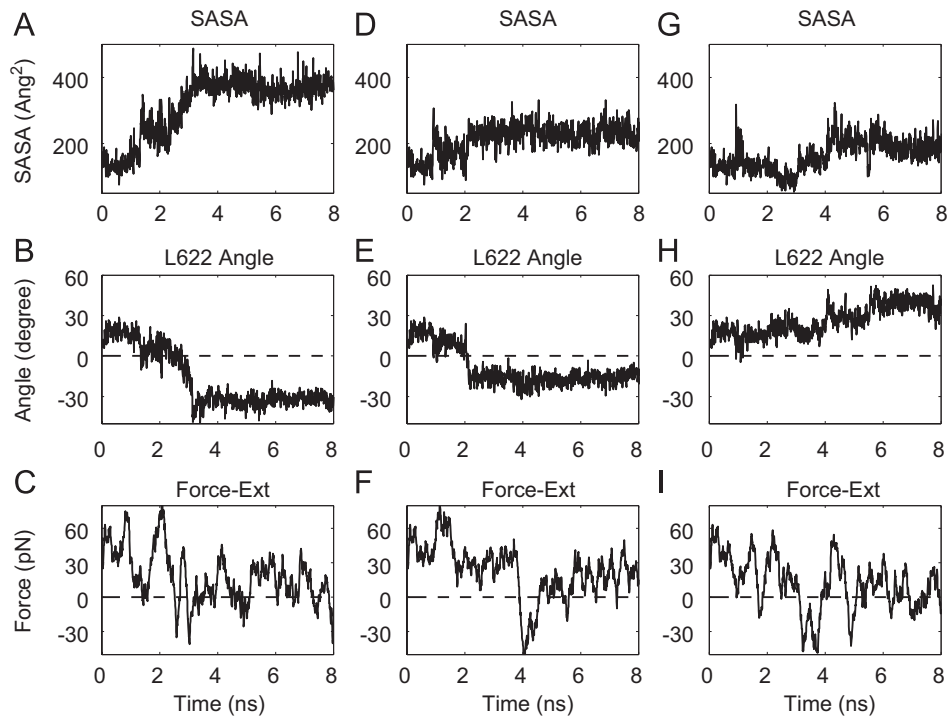


Fig. 4. Results from three TAL5 simulations: from two simulations undergoing VBS1 activation (A)–(C) and (D)–(F), and also from a simulation without activation (G)–(I). (A), (D), (G) Change in SASA of hydrophobic (red) and polar (blue) residues of VBS1. (B), (E), (H) Angle of rotation of VBS1 relative to H5 (defined in Supplementary Fig. S1). Positive angle corresponds to the inactive state of VBS1, and negative angles correspond to activation. (C), (F), (I) Force applied to TAL5.

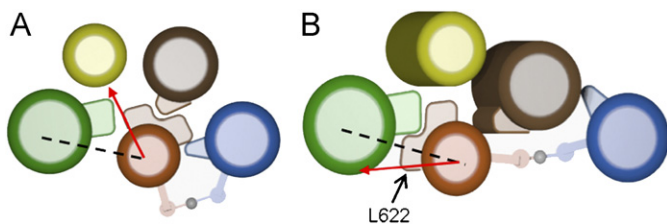


Fig. 5. The angle of VBS1 rotation is defined by the angle formed between L622 of VBS1 and a vector connecting the centers of mass of VBS1 and H5. (A) Before force application, the angle is positive with L622 inside the hydrophobic core. (B) After forcing, the angle is negative with L622 outside the hydrophobic core.

Karplus, 1999). Other implicit solvent methods (Schaefer et al., 2001; Im et al., 2003) are theory based, and they are 5–10 times slower than EEF1. EEF1 has been demonstrated to produce reasonable MD trajectories (Lazaridis and Karplus, 1999; Paci and Karplus, 2000; Brockwell et al., 2003). To verify the validity of the EEF1 results, a constant velocity simulation with an effective pulling rate of 0.5 \AA/ns and a constant force simulation with $F = 50.0 \text{ pN}$ were performed on TAL5 with explicit solvent. In both explicit simulations, RQK and ER handles formed persistent hydrogen bonds with H1, and the vinculin-binding surfaces of VBS1 became partially exposed in the 3.2 ns constant velocity simulation or the 1.6 ns constant force simulation (Fig. 7). Explicit water molecules are known to slow diffusion-like transitions in proteins, and require much longer simulation times than

the implicit simulations (8 ns) to obtain similar range in motion. Full rotation of VBS1 therefore was not observed. The critical factors in VBS1 activation in EEF1 simulations are strong VBS1–H1 interaction, applied torque through RQK and ER handles, and disruption of VBS1–H5 hydrophobic interaction. In both the constant velocity simulation ($10.58 \pm 0.25 \text{ \AA}$) and the constant force simulation ($11.03 \pm 0.22 \text{ \AA}$), the average distances between VBS1 and H5 are clearly larger than the ones observed in the non-forced simulations (Table 1).

It is important to recognize that the conformational changes critically depend on the manner and direction in which the force is applied (Brockwell et al., 2003; Li and Makarov, 2004; Vogel, 2006). Previous MD simulations have generally pulled on the N- and C-termini, and the results are often domain unfolding; e.g. (Lu et al., 1998; Gao et al., 2002). Complete unfolding is rarely observed in normal protein binding, however, so there is no reason a priori to expect that it would be necessary for force-induced reactions. We have attempted to apply a force in a realistic direction that mimics the force transmission within talin. Adjacent secondary structures of a protein commonly interact by forming hydrophobic contacts and hydrogen bonds around the hydrophobic patch. Applied forces, therefore, are likely transmitted through the hydrogen bonds between the secondary structures (Lu et al., 1998; Gao et al., 2002). The notable difference of pulling in this study compared to other unfolding simulations is that we apply the force on the hydrogen-bonding residues, which is

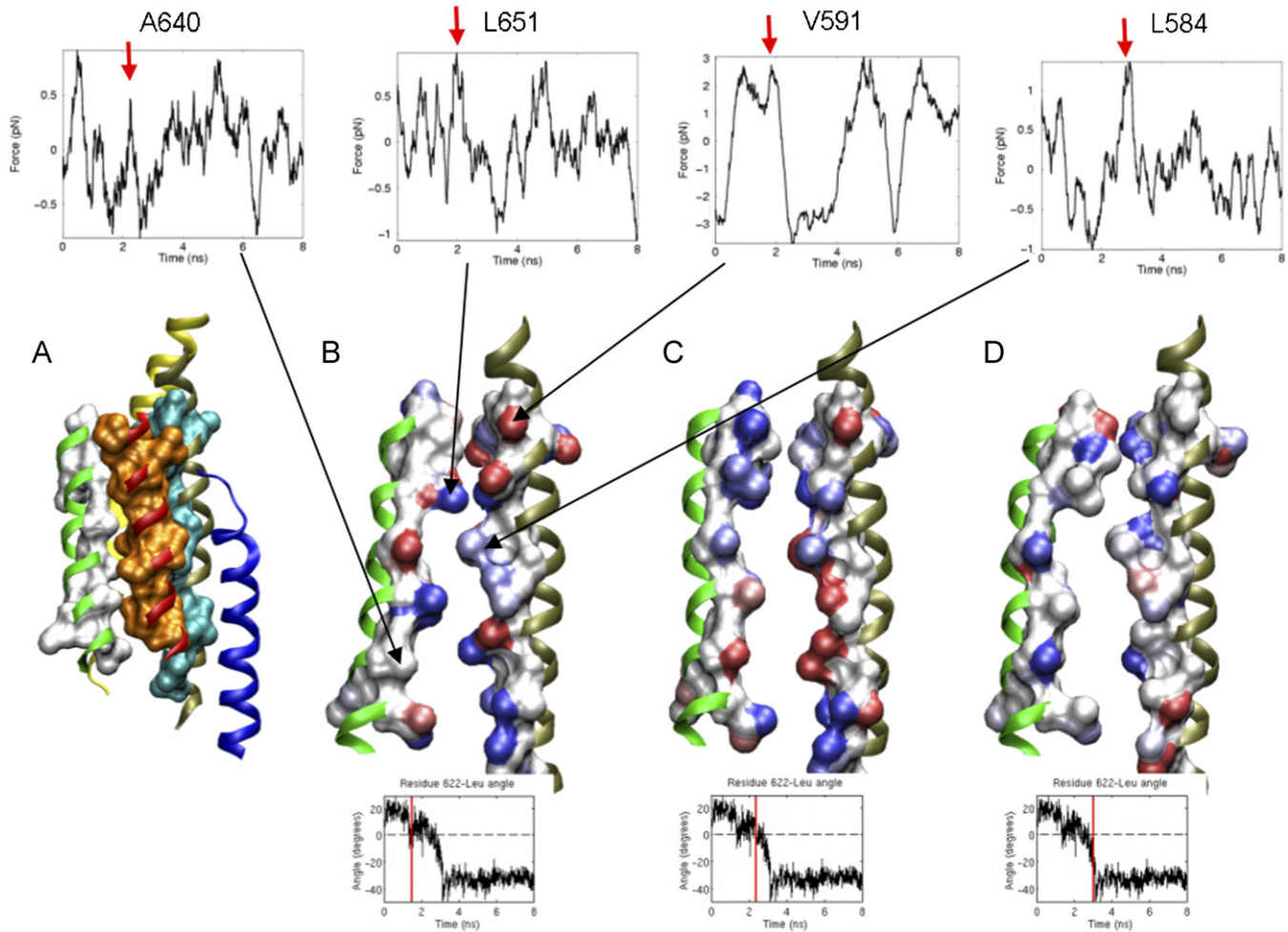


Fig. 6. (A) TAL5 in the same orientation and color coding as in Fig. 2A. (B) Only H3 and H5 are shown in the same orientation as in (A) at $t = 1.52$ ns to highlight the force magnitude exerted on the hydrophobic residues by the hydrophobic residues of VBS1 (not shown for clarity) with force magnitude below the average force in blue, near average in white, and above average in red. Residues shown in red are opposing VBS1 rotation. Once the hydrophobic residues slip, corresponding force drops are as shown in blue. The snap incident is indicated on the VBS1 rotation plot (Fig. 4B) as a red vertical line. Time traces of force magnitude are shown for A640, L651, L584, and V591 in the subset. Force peaks near 2 ns are indicated by red arrows, which correspond to events in which the hydrophobic contacts yield to VBS1 rotation. (C) Forces on hydrophobic sidechains at $t = 2.40$ ns just before slip of hydrophobic residues yielding to VBS1 rotation. (D) Forces on hydrophobic side chains at $t = 3.04$ ns after the hydrophobic slip and corresponding force drops.

a likely site of force transmission between secondary structures, rather than on the two termini. Since the pulling direction is primarily determined by the relative locations of force application sites and fixed points, in choosing to apply force to the polar residues of H1, and to fix the polar residues of H5, forces tend to be directed nearly perpendicular to the TAL5 principle axis (Fig. 1B). VBS1 activation was found to be somewhat dependent upon the sites of force application and, consequently, on the direction of pulling (data not shown). However, given what is currently known about the structure of talin, and the probable sites of interaction with neighboring domains of the protein, these assumptions seemed reasonable.

The force extension curves have the typical sawtooth shape (Fig. 4C, F, and I) with the force-drops corresponding to rupture of the hydrogen bonds or slippage of hydrophobic contacts between secondary structures, which

are similarly observed in other AFM and MD studies (Marszalek et al., 1999; Carrion-Vazquez et al., 2003). Thus, VBS1 activation occurs through rotation of VBS1 relative to the TAL5, as a consequence of torque applied via hydrogen bonds and salt bridges between H1 and VBS1. Thus, the conformational change required for activation is subtle, involving an extension of less than 2 Å and no domain unfolding, as has been found in the activation of other cryptic sites, such as fibronectin (Gao et al., 2002).

The potential of mean force (PMF), or free energy landscape along the extension, has a monotonically increasing profile without any apparent local minima (Kirmizialtin et al., 2005), suggesting that the zero force structure resides in the global minimum (Fig. 8). There is, however, a region of decreased slope on the PMF curve near extension of $x = 1.4$ Å that corresponds to the

hydrophobic slip of VBS1. Activation can be interpreted in the context of the PMF curve representing the free energy change along a specified reaction coordinate in the absence of force (Kirmizialtin et al., 2005). The plateau at $x = 1.4 \text{ \AA}$ becomes a local minimum when the molecule is exposed to a force as low as 20.0 pN, allowing it to undergo the conformational change (Kirmizialtin et al., 2005; Karcher et al., 2006). This is reflected, for example, by an increased probability of 50% in the activated state under a force of 20.0 pN compared to a zero force case. An extended state from one of the simulations with VBS1 hydrophobic residues partially exposed was used in a relaxation explicit water simulation for about 1 ns with all the constraints removed. In the absence of force, the exposed hydrophobic

residues rotated back into the hydrophobic core indicating that the non-extended state indeed is the global minimum (Fig. 9) and that de-activation occurs almost immediately following the release of force.

Varying magnitudes of force are applied to TAL5 during the constant velocity simulations as VBS1 undergoes activation (Fig. 4C, F, and I). Although the peak magnitude applied through TAL5 is $55.4 \pm 19.1 \text{ pN}$, the mean force applied throughout the simulations is $13.2 \pm 8.0 \text{ pN}$. In order to verify this finding, constant force simulations were performed. All constant force simulations ($n = 8$) with force magnitude $\geq 18.0 \text{ pN}$ underwent VBS1 activation, whereas all simulations ($n = 4$) with forces $\leq 17.0 \text{ pN}$ did not (data not shown). The effective pulling rate of 0.125 \AA/ns is still many orders of magnitude faster than the pulling rates we might expect in vivo or with AFM experiments ($\sim 1 \text{ nm/ms}$ or 10^{-5} \AA/ns). Such rapid pulling results in significantly larger force levels in bond rupture (Evans and Ritchie, 1997) or protein unfolding (Hummer and Szabo, 2003) compared to the corresponding AFM measurements. In both cases, the forces measured by AFM were $\sim 30\%$ of the force computed using MD (Evans and Ritchie, 1997; Hummer and Szabo, 2003). Using this value as a very rough approximation, the force needed to activate VBS1 ($13.2 \pm 8.0 \text{ pN}$) at more realistic, slower rates of pulling would lie in the range of $\sim 4 \text{ pN}$. This estimated lower force at slower pulling rate is on the order of (i) forces generated by a single myosin, $\sim 4 \text{ pN}$ (Finer et al., 1995); (ii) forces needed to rupture a talin-F-actin bond, $\sim 2 \text{ pN}$ (Jiang et al., 2003); and (iii) the estimated force experienced by a single integrin linkage, based on close packing in a focal contact, $\sim 1 \text{ pN}$ (Balaban et al., 2001). On the extracellular side, the force required to break a single integrin-fibronectin bond is $\sim 20 \text{ pN}$ (Thoumine and Meister, 2000), and a single integrin-fibrinogen bond can withstand $\sim 100 \text{ pN}$ (Litvinov et al., 2002).

In conclusion, we identify a potential mechanism for VBS1 activation, involving a force-induced conformational change causing the hydrophobic vinculin-binding residues

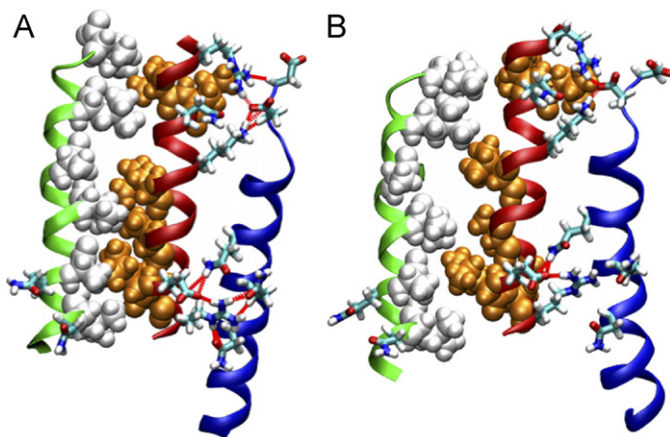


Fig. 7. Two conformations from a constant force ($F = 50.0 \text{ pN}$) explicit water simulation. (A) Conformation at $t = 0.112 \text{ ns}$ and (B) conformation at $t = 1.2 \text{ ns}$. The simulation lasted 1.6 ns. The hydrophobic residues of VBS1 seem to be beginning to expose to solvent. Although VBS1 rotation is much smaller in extent compared to those measured in the implicit solvent simulation, VBS1 still has very strong hydrogen-bonding interactions with H1, where the torque applied through transmitted force. Trajectory from constant velocity simulation in explicit solvent (3.2 ns in duration) also show strong interaction between VBS1 and H1, but VBS1 rotation is not observed to the same extent as in the implicit solvent simulations.

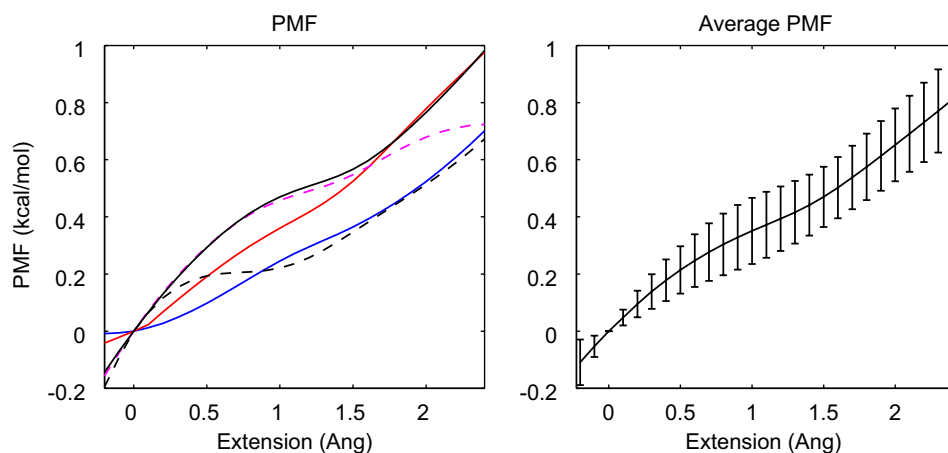


Fig. 8. (Left) Calculated potential mean force (PMF) curves from TAL5 simulations ($n = 5$). Each PMF is shifted vertically so that the mean value for each is zero. (Right) Averaged PMF.

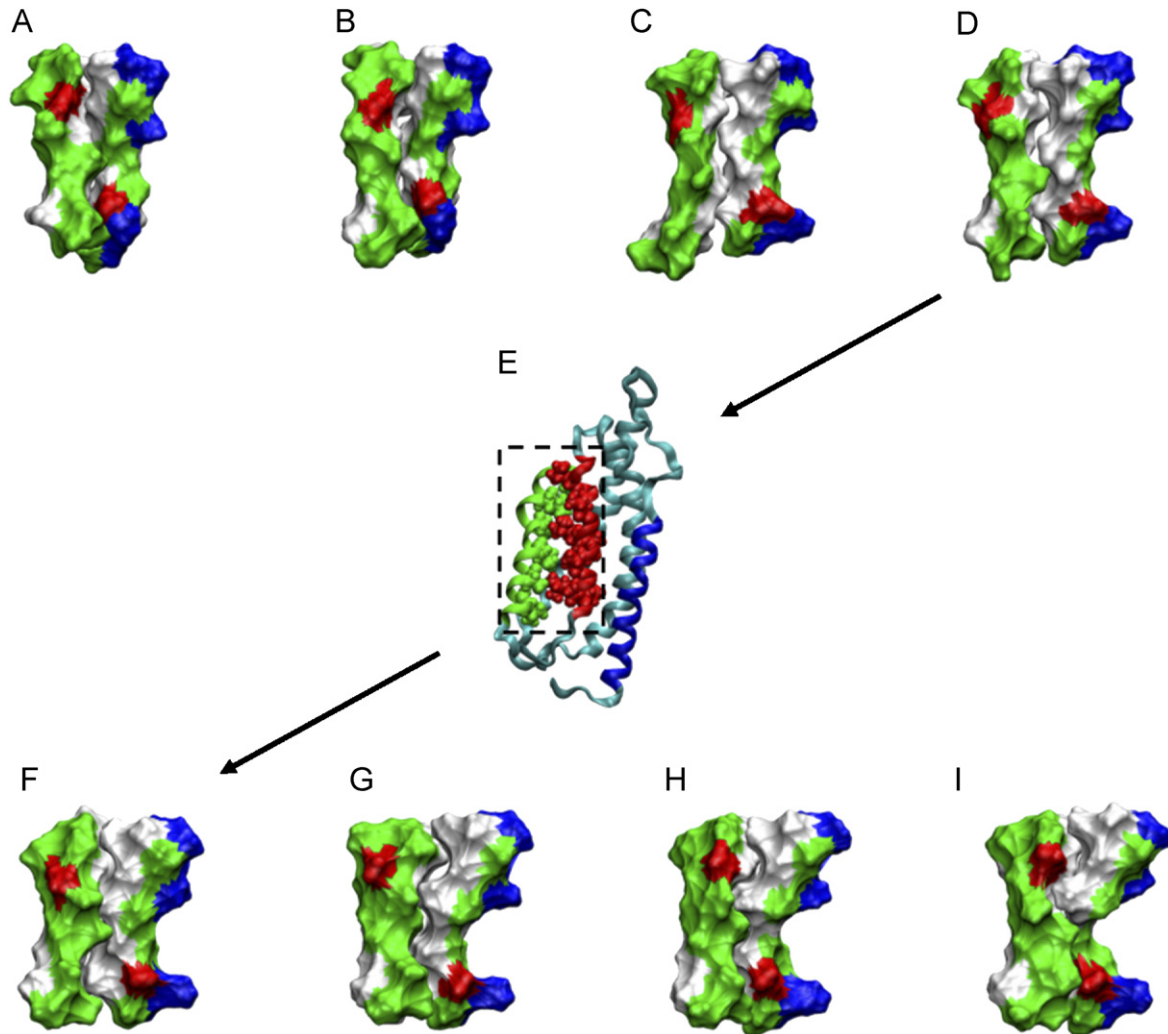


Fig. 9. Surface representation of VBS1 and H5 from the TAL9 simulation at (A) $t = 0$ ns, (B) $t = 5.12$ ns, (C) $t = 10.24$ ns, and (D) $t = 15.36$ ns. Hydrophobic residues are shown in white, polar residues in green, negative residues in red and positive residues in blue. These views show that the hydrophobic residues of VBS1 are partially exposed to the solvent. (E) The ribbon representation of TAL5 at $t = 15.36$ ns is shown with H1 in blue ribbon, H4 in red ribbon, H5 in green ribbon, VBS1 hydrophobic residues in red VDW, and H5 hydrophobic residues in green VDW. The dotted box indicates that the surface representations are only showing VBS1 and H5. The extended TAL9 at $t = 15.36$ ns is truncated to TAL5, solvated in rhombic dodecahedron water-box, removed all external forces, and simulated for slightly longer than 1 ns. The configurations at (F) $t = 0$ ps, (G) $t = 352$ ps, (H) $t = 704$ ps, and (I) $t = 1056$ ps of the relaxing dynamics show that the exposed hydrophobic residues return to their cryptic conformation.

on VBS1 within TAL5 to become accessible for vinculin binding. This would then constitute the initiating event leading to force-induced focal adhesion strengthening by vinculin recruitment.

Acknowledgements

We gratefully acknowledge support from the NIH (HL064858) (GM076689), the Gates Millennium Scholarship and Computational Science Graduate Fellowship from Department of Energy (to S. Lee) as well as the NSF through the San Diego Supercomputer Center under Grant MCB050050S using SDSC DataStar IBM p655. We also thank Dr. Sid Chung for his assistance in creating the 3D models of TAL5.

Appendix A. Supplementary data

The online version of this article contains additional supplementary data. Please visit [doi:10.1016/j.jbiomech.2007.04.006](https://doi.org/10.1016/j.jbiomech.2007.04.006).

References

- Bakolitsa, C., de Pereda, J.M., Bagshaw, C.R., Critchley, D.R., Liddington, R.C., 1999. Crystal structure of the vinculin tail suggests a pathway for activation. *Cell* 99 (6), 603–613.
- Balaban, N.Q., Schwarz, U.S., Rivelino, D., Goichberg, P., Tzur, G., Sabanay, I., Mahalu, D., Safran, S., Bershadsky, A., Addadi, L., Geiger, B., 2001. Force and focal adhesion assembly: a close relationship studied using elastic micropatterned substrates. *Nature Cell Biology* 3 (5), 466–472.

- Bass, M.D., Smith, B.J., Prigent, S.A., Critchley, D.R., 1999. Talin contains three similar vinculin-binding sites predicted to form an amphipathic helix. *Biochemical Journal* 341, 257–263.
- Beck, D.A., Armen, R.S., Daggett, V., 2005. Cutoff size need not strongly influence molecular dynamics results for solvated polypeptides. *Biochemistry* 44 (2), 609–616.
- Bois, P.R., Borgon, R.A., Vornrhein, C., Izard, T., 2005. Structural dynamics of alpha-actinin-vinculin interactions. *Molecular Cell Biology* 25 (14), 6112–6122.
- Brockwell, D.J., Paci, E., Zinober, R.C., Beddard, G.S., Olmsted, P.D., Smith, D.A., Perham, R.N., Radford, S.E., 2003. Pulling geometry defines the mechanical resistance of a beta-sheet protein. *Nature Structural Biology* 10 (9), 731–737.
- Brooks, B.R., Brucoleri, R.E., Olafson, B.D., States, D.J., Swaminathan, S., Karplus, M., 1983. Charmm—a program for macromolecular energy, minimization, and dynamics calculations. *Journal of Computational Chemistry* 4 (2), 187–217.
- Calderwood, D.A., 2004. Talin controls integrin activation. *Biochemical Society Transactions* 32, 434–437.
- Carrion-Vazquez, M., Li, H., Lu, H., Marszalek, P.E., Oberhauser, A.F., Fernandez, J.M., 2003. The mechanical stability of ubiquitin is linkage dependent. *Nature Structural Biology* 10 (9), 738–743.
- Critchley, D.R., 2000. Focal adhesions—the cytoskeletal connection. *Current Opinion in Cell Biology* 12 (1), 133–139.
- Di Paolo, G., Pellegrini, L., Letinic, K., Cestra, G., Zoncu, R., Voronov, S., Chang, S., Guo, J., Wenk, M.R., De Camilli, P., 2002. PI(4,5)P2 generation at sites of cell adhesion: recruitment and regulation of PIP kinase type Igamma by the FERM domain of talin. *Molecular Biology of the Cell* 13, 337A.
- Evans, E., Ritchie, K., 1997. Dynamic strength of molecular adhesion bonds. *Biophysical Journal* 72 (4), 1541–1555.
- Feig, M., Karanicolas, J., Brooks 3rd, C.L., 2004. MMTSB Tool Set: enhanced sampling and multiscale modeling methods for applications in structural biology. *Journal of Molecular Graphics and Modelling* 22 (5), 377–395.
- Finer, J.T., Mehta, A.D., Spudich, J.A., 1995. Characterization of single actin-myosin interactions. *Biophysical Journal* 68 (4 Suppl), 291S–296S ; discussion 296S–297S.
- Galbraith, C.G., Yamada, K.M., Sheetz, M.P., 2002. The relationship between force and focal complex development. *Journal of Cell Biology* 159 (4), 695–705.
- Gao, M., Craig, D., Vogel, V., Schulten, K., 2002. Identifying unfolding intermediates of FN-III(10) by steered molecular dynamics. *Journal of Molecular Biology* 323 (5), 939–950.
- Giannone, G., Jiang, G., Sutton, D.H., Critchley, D.R., Sheetz, M.P., 2003. Talin1 is critical for force-dependent reinforcement of initial integrin-cytoskeleton bonds but not tyrosine kinase activation. *Journal of Cell Biology* 163 (2), 409–419.
- Gingras, A.R., Vogel, K.P., Steinhoff, H.J., Ziegler, W.H., Patel, B., Emsley, J., Critchley, D.R., Roberts, G.C., Barsukov, I.L., 2006. Structural and dynamic characterization of a vinculin binding site in the talin rod. *Biochemistry* 45 (6), 1805–1817.
- Hemmings, L., Rees, D.J.G., Ohanian, V., Bolton, S.J., Gilmore, A.P., Patel, B., Priddle, H., Trevithick, J.E., Hynes, R.O., Critchley, D.R., 1996. Talin contains three actin-binding sites each of which is adjacent to a vinculin-binding site. *Journal of Cell Science* 109, 2715–2726.
- Hoover, W.G., 1985. Canonical dynamics: equilibrium phase-space distributions. *Physical Review A* 31 (3), 1695–1697.
- Hummer, G., Szabo, A., 2003. Kinetics from nonequilibrium single-molecule pulling experiments. *Biophysical Journal* 85 (1), 5–15.
- Im, W., Lee, M.S., Brooks 3rd, C.L., 2003. Generalized born model with a simple smoothing function. *Journal of Computational Chemistry* 24 (14), 1691–1702.
- Izard, T., Evans, G., Borgon, R.A., Rush, C.L., Bricogne, G., Bois, P.R.J., 2004. Vinculin activation by talin through helical bundle conversion. *Nature* 427 (6970), 171–175.
- Izrailev, S., Crofts, A.R., Berry, E.A., Schulten, K., 1999. Steered molecular dynamics simulation of the Rieske subunit motion in the cytochrome bc(1) complex. *Biophysical Journal* 77 (4), 1753–1768.
- Jiang, G.Y., Giannone, G., Critchley, D.R., Fukumoto, E., Sheetz, M.P., 2003. Two-piconewton slip bond between fibronectin and the cytoskeleton depends on talin. *Nature* 424 (6946), 334–337.
- Kamm, R.D., Kaazempur-Mofrad, M.R., 2004. On the molecular basis for mechanotransduction. *Mechanics and Chemistry of Biosystems* 1 (3), 201–209.
- Karcher, H., Lee, S.E., Kaazempur-Mofrad, M.R., Kamm, R.D., 2006. A coarse-grained model for force-induced protein deformation and kinetics. *Biophysical Journal* 90 (8), 2686–2697.
- Kirmizialtin, S., Huang, L., Makarov, D.E., 2005. Topography of the free-energy landscape probed via mechanical unfolding of proteins. *Journal of Chemical Physics* 122 (23), 234915.
- Krautner, V., Van Gunsteren, W.F., Hunenberger, P.H., 2001. A fast SHAKE: algorithm to solve distance constraint equations for small molecules in molecular dynamics simulations. *Journal of Computational Chemistry* 22 (5), 501–508.
- Lazaridis, T., Karplus, M., 1999. Effective energy function for proteins in solution. *Proteins* 35 (2), 133–152.
- Li, P.C., Makarov, D.E., 2004. Simulation of the mechanical unfolding of ubiquitin: probing different unfolding reaction coordinates by changing the pulling geometry. *Journal of Chemical Physics* 121 (10), 4826–4832.
- Ling, K., Doughman, R.L., Firestone, A.J., Bunce, M.W., Anderson, R.A., 2002. Type I gamma phosphatidylinositol phosphate kinase targets and regulates focal adhesions. *Nature* 420 (6911), 89–93.
- Litvinov, R.I., Shuman, H., Bennett, J.S., Weisel, J.W., 2002. Binding strength and activation state of single fibrinogen-integrin pairs on living cells. *Proceedings of the National Academy of Sciences of the United States of America* 99 (11), 7426–7431.
- Lu, H., Isralewitz, B., Krammer, A., Vogel, V., Schulten, K., 1998. Unfolding of titin immunoglobulin domains by steered molecular dynamics simulation. *Biophysical Journal* 75 (2), 662–671.
- MacKerell, A., Bashford, D., Bellott, M., Dunbrack, R., Evanseck, J., Field, M., Fischer, S., Gao, J., Guo, H., Ha, S., et al., 1998. All-atom empirical potential for molecular modeling and dynamics studies of proteins. *Journal of Physical Chemistry* 102, 3586–3616.
- Marszalek, P.E., Lu, H., Li, H., Carrion-Vazquez, M., Oberhauser, A.F., Schulten, K., Fernandez, J.M., 1999. Mechanical unfolding intermediates in titin modules. *Nature* 402 (6757), 100–103.
- Neria, E., Fischer, S., Karplus, M., 1996. Simulation of activation free energies in molecular dynamics system. *Journal of Chemical Physics* 105, 1902–1921.
- Nosé, S., 1984. A molecular dynamics method for simulations in the canonical ensemble. *Molecular Physics* 52, 255–268.
- Oberhauser, A.F., Badilla-Fernandez, C., Carrion-Vazquez, M., Fernandez, J.M., 2002. The mechanical hierarchies of fibronectin observed with single-molecule AFM. *Journal of Molecular Biology* 319 (2), 433–447.
- Paci, E., Karplus, M., 2000. Unfolding proteins by external forces and temperature: the importance of topology and energetics. *Proceedings of the National Academy of Sciences of the United States of America* 97 (12), 6521–6526.
- Papagrigoriou, E., Gingras, A.R., Barsukov, I.L., Bate, N., Fillingham, I.J., Patel, B., Frank, R., Ziegler, W.H., Roberts, G.C.K., Critchley, D.R., Emsley, J., 2004. Activation of a vinculin-binding site in the talin rod involves rearrangement of a five-helix bundle. *EMBO Journal* 23 (15), 2942–2951.
- Patel, B.C., Gingras, A.R., Bobkov, A.A., Fujimoto, L.M., Zhang, M., Liddington, R.C., Mazzeo, D., Emsley, J., Roberts, G.C., Barsukov, I.L., Critchley, D.R., 2006. The activity of the vinculin binding sites in talin is influenced by the stability of the helical bundles that make up the talin rod. *Journal of Biological Chemistry*.
- Priddle, H., Hemmings, L., Monkley, S., Woods, A., Patel, B., Sutton, D., Dunn, G.A., Zicha, D., Critchley, D.R., 1998. Disruption of the talin gene compromises focal adhesion assembly in undifferentiated but not differentiated embryonic stem cells. *Journal of Cell Biology* 142 (4), 1121–1133.

- Schaefer, M., Bartels, C., Leclerc, F., Karplus, M., 2001. Effective atom volumes for implicit solvent models: comparison between Voronoi volumes and minimum fluctuation volumes. *Journal of Computational Chemistry* 22 (15), 1857–1879.
- Sotomayor, M., Schulten, K., 2004. Molecular dynamics study of gating in the mechanosensitive channel of small conductance MscS. *Biophysical Journal* 87 (5), 3050–3065.
- Thoumine, O., Meister, J.J., 2000. Dynamics of adhesive rupture between fibroblasts and fibronectin: microplate manipulations and deterministic model. *European Biophysics Journal* 29 (6), 409–419.
- Torrie, G. M., J.P.V., 1974. Monte carlo free energy estimates using non-boltzmann sampling: Application to the sub-critical lennard-jones fluid. *Chemical Physics Letters* 28, 578–581.
- Vogel, V., 2006. Mechanotransduction involving multimodular proteins: converting force into biochemical signals. *Annual Review of Biophysics and Biomolecular Structure* 35, 459–488.
- Vogel, V., Sheetz, M., 2006. Local force and geometry sensing regulate cell functions. *Nature Reviews Molecular Cell Biology* 7 (4), 265–275.
- Winkler, J., Lunsdorf, H., Jockusch, B.M., 1996. The ultrastructure of chicken gizzard vinculin as visualized by high-resolution electron microscopy. *Journal of Structural Biology* 116 (2), 270–277.
- Xing, B.D., Jedsadayanmata, A., Lam, S.C.T., 2001. Localization of an integrin binding site to the C terminus of talin. *Journal of Biological Chemistry* 276 (48), 44373–44378.
- Xu, W.M., Coll, J.L., Adamson, E.D., 1998. Rescue of the mutant phenotype by reexpression of full-length vinculin in null F9 cells; effects on cell locomotion by domain deleted vinculin. *Journal of Cell Science* 111, 1535–1544.
- Ylanne, J., Scheffzek, K., Young, P., Saraste, M., 2001. Crystal structure of the alpha-actinin rod reveals an extensive torsional twist. *Structure* 9 (7), 597–604.